Kinetic Monte Carlo simulations compared with continuum models and experimental properties of pattern formation during ion beam sputtering

2009 J. Phys.: Condens. Matter 21 224016

(http://iopscience.iop.org/0953-8984/21/22/224016)

IOP Publishing Journal of Physics: Condensed Matter

J. Phys.: Condens. Matter **21** (2009) 224016 (12pp) doi:10.1088/0953-8984/21/22/224016

Kinetic Monte Carlo simulations compared with continuum models and experimental properties of pattern formation during ion beam sputtering

E Chason[1] **and W L Chan**[2]

[1] Brown University, Division of Engineering, Providence, RI 02192, USA
[2] University of Illinois at Urbana-Champaign, Urbana, IL 61801, USA

E-mail: Eric_Chason@Brown.edu and WLChan@uiuc.edu

Received 28 November 2008
Published 12 May 2009
Online at stacks.iop.org/JPhysCM/21/224016

Abstract

Kinetic Monte Carlo simulations model the evolution of surfaces during low energy ion bombardment using atomic level mechanisms of defect formation, recombination and surface diffusion. Because the individual kinetic processes are completely determined, the resulting morphological evolution can be directly compared with continuum models based on the same mechanisms. We present results of simulations based on a curvature-dependent sputtering mechanism and diffusion of mobile surface defects. The results are compared with a continuum linear instability model based on the same physical processes. The model predictions are found to be in good agreement with the simulations for predicting the early-stage morphological evolution and the dependence on processing parameters such as the flux and temperature. This confirms that the continuum model provides a reasonable approximation of the surface evolution from multiple interacting surface defects using this model of sputtering. However, comparison with experiments indicates that there are many features of the surface evolution that do not agree with the continuum model or simulations, suggesting that additional mechanisms are required to explain the observed behavior.

1. Introduction

Ion-beam-induced nanopatterning has been studied for the past 40 years [1–4], yet there are still fundamental questions about the mechanisms that control it. The wide array of observed behavior illustrates the complex phenomena that can occur from the interaction of a few basic surface processes such as sputtering, defect generation and surface diffusion. This complexity, however, makes it difficult to determine the mechanisms that control it and even further difficult to predict the surface evolution.

A primary approach for understanding the morphology evolution has been to develop continuum equations for the surface evolution based on different physical mechanisms, e.g., the dependence of the sputter yield on the local morphology [5] or barriers to diffusion of defects over step edges (referred to as ES barriers) [2]. In this work, we focus primarily on the effects of the morphology-dependent sputter yield (some effects due to ES barriers are discussed in section 4.6). This mechanism has lead to increasingly sophisticated analytical models of the surface evolution, starting with a simple linear instability model [5] and then extended to include non-linear interactions [1, 6–8] and coupling between the morphology and surface defects [9]. These models have had considerable success in elucidating the kinetic regimes of patterning [3] and developing physical mechanisms to account for different observations.

A major challenge of the continuum approach is developing differential equations that account for the surface evolution resulting from a large number of interacting particles. An alternative approach is to simulate the kinetic behavior at the atomic level rather than capturing the overall evolution with analytical expressions. This approach can be implemented in a number of ways, including kinetic Monte Carlo (KMC)

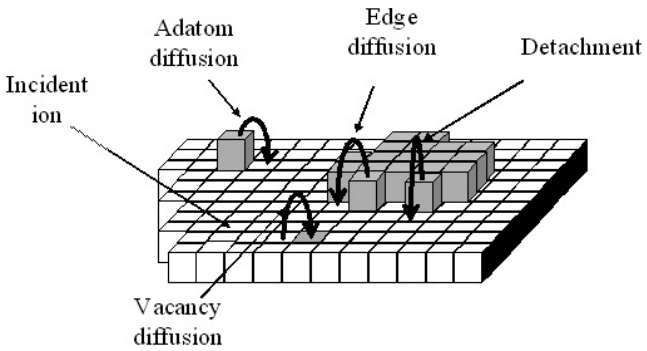

Figure 1. Example of transitions related to some of the surface kinetic processes modeled in the KMC simulation. The rate of hopping is determined by an activation energy that depends on the initial configuration and the final configuration. This allows vacancies to diffuse on the surface with the same rate as adatoms.

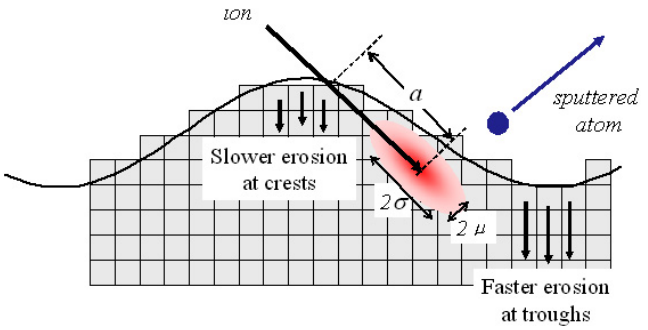

Figure 2. Schematic representation of the sputtering process used in the simulations based on the Sigmund model.
(This figure is in colour only in the electronic version)

methods such as the one described in this article. The evolution of the surface then arises from allowing the individual particles to act according to these rules without an *a priori* understanding of how this behavior will occur. In this respect, continuum models and simulations are complementary in that they are both ways of predicting the surface evolution under the action of different physical mechanisms.

In the following article, we describe a simple KMC model [10] that we have developed for simulating the evolution of surfaces during low energy ion sputtering. Because we specify precisely all the mechanisms that go into the KMC simulations, we can compare the results directly with the prediction of continuum theories based on these mechanisms. The degree of agreement/disagreement between the two helps to determine whether they are good analytical models of the surface evolution due to these mechanisms. We also compare the simulation and continuum predictions with experiments to determine where the models are insufficient to explain the observed behavior and discuss other mechanisms that may need to be included.

2. KMC approach

Surface evolution is modeled in the KMC approach by assigning rates to different surface processes (shown schematically in figure 1) and executing events on the surface with a probability proportional to their relative rates [10, 11]. The surface is modeled as a square lattice and uses a solid-on-solid model so that there is only one surface site associated with each lattice site (no overhangs are allowed). The surface processes that we include are based on physical mechanisms that have been previously proposed in continuum theories of ripple formation, i.e., ion-induced sputtering and surface diffusion of surface defects. The KMC model is described more fully in [10], so only a brief description is given here.

The sputtering is based on a mechanism proposed by Sigmund [12, 13] which models the distribution of energy deposited by an ion into the surface region as it undergoes nuclear collisions. Shown schematically in cross-section in figure 2, the energy distribution is modeled as a Gaussian centered at a distance a from the point where the ion enters the surface with widths of μ and σ in the directions parallel and perpendicular to the incident ion direction. This is intended to model the average over a large number of incident ions rather than the effect of a single ion impact. The probability of sputtering an atom from a site on the surface is taken to be proportional to the average energy deposited at that site according to the Sigmund distribution function.

In the KMC, sputtering is modeled by the action of individual ions impinging on a surface consisting of discrete sites. An incident ion is simulated by randomly choosing a trajectory with the proper incident angle and calculating the point of impact on the surface. The energy deposited at each surface site is then calculated based on the Sigmund energy distribution. The site for sputter removal of an atom is chosen probabilistically based on the relative energy deposition at each surface site. This process is repeated if necessary to achieve the proper average sputter yield. Note that this differs from the continuum approach (described below) in that the surface height is changed only at the site where the sputtering occurs in units of whole atoms. In contrast, the continuum approach treats the surface as a smooth function (represented by the solid sinusoidal line in figure 2). The Sigmund process leads to a sputter yield that depends on the surface curvature and the surface changes incrementally over many sites due to the sputtering.

Removal of atoms by the sputtering process in the simulation leads to the creation of surface vacancies with a rate that depends on the local surface morphology. This ignores the creation of other defects such as subsurface interstitials and vacancies that can be created by the ion-induced displacements. This can be true at high temperature where most of the defects recombine [14] so that only the vacancies created by the sputtering of atoms will remain. Similarly, the continuum theories also only model the removal of atoms from the surface by sputtering and ignore the creation of other defects. Still, it is worth noting that the defect formation in real systems may be different than the approximation made by the Sigmund mechanism. It has also been pointed out that there may be significant rearrangement of atoms on the surface due to the incident ion which may lead to different behavior than predicted by the Sigmund model [15–17]. These issues will be discussed more below.

The other process that contributes to surface evolution is diffusion of adatoms and vacancies on the surface. The probability of an atom hopping from one site (i) to another (j) is determined by the transition rate between different sites on the surface, given by $\Gamma \exp(-\Delta E_{i,j}/kT)$ where Γ is an attempt frequency and $\Delta E_{i,j}$ is an activation energy that depends on the coordination of the initial (n_i) and final (n_j) site. If the coordination decreases in the transition, an additional energetic barrier of $(n_i - n_j)E_b$ is added to account for the effect of breaking bonds. This ensures that detailed balance is preserved in the simulation.

Transitions between different coordination states are associated with different configurations on the surface (some examples are shown in figure 1) and the energetic barriers for each type of transition are specified individually in the simulation. For example, transitions from a site with zero coordination to another with zero coordination corresponds to the process of adatom diffusion. Detachment from the step edge decreases the coordination from one to zero so there is an additional energetic barrier to this motion. The motion of an atom from a 3-coordinated site to another 3-coordinated site corresponds to the diffusion of a vacancy on the surface. Even though the initial site has large coordination, the transition energy does not have to be large because there are no bonds broken, i.e., the final coordination is the same as the initial coordination. For this reason, surface vacancies in our simulation are given the same high mobility as adatoms, consistent with experimental results on Cu(001) surfaces [18]. For the simulation results presented below, ΔE_{ij} is taken to be 0.8 eV for most of the transitions and E_b is equal to 0.2 eV; further details can be found in [10].

Using the rates described above, we execute surface processes at different sites with probabilities based on their relative rates. By summing the transition rates of all the active surface sites, we can also calculate the total rate (R) of all processes occurring on the surface We associate a time step of $\Delta t = 1/R$ with each event on the surface so that the simulated time can be accurately calculated with respect to the surface morphology evolution. After executing an event on the surface, we update all the configurations and transition rates and then repeat the process to simulate the evolving morphology on the surface.

Other Monte Carlo simulations of surface evolution during sputtering use approaches that differ in various ways from the one described above. Cuerno *et al* [19] used a morphology-dependent sputter yield and Koponen [20] used the binary collision approximation to model the sputter yield, but these works did not use thermally-activated hopping to model the defect kinetics. Other simulations using the Sigmund mechanism [21–24] for sputtering have modeled thermally-activated defect kinetics in different ways but did not include the motion of surface vacancies. These works all showed the formation of ripples aligned with the ion direction, though the different models of defect motion make it difficult to compare the results of the different studies. Other works [25–28] modeled the effects of mobile defects but did not include a morphology-dependent sputter yield of the type included in the Sigmund mechanism. These works were focused primarily on understanding pattern formation produced by ES barriers to diffusion over step edges rather than on the type of ripples based on the Sigmund mechanism.

3. Continuum theories in the linear instability regime

The first continuum theory of ripple formation was derived by Bradley and Harper (BH) [5] who considered the combined effects of sputtering and surface diffusion on the evolution of the surface height. They calculated how the Sigmund sputtering mechanism affected the entire surface profile and showed that it resulted in a sputter yield that is proportional to the curvature of the surface $(v_x \partial^2 h/\partial x^2 + v_y \partial^2 h/\partial y^2)$ where $x(y)$ refers to the direction on the surface parallel (perpendicular) to the ion beam. For a surface with a sinusoidal profile, this means that the crests of the waves on the surface sputter slower than the troughs, leading to surfaces that become rougher as they are sputtered. This roughening mechanism is balanced by surface diffusion which depends on the divergence of the surface curvature $(-B\partial^4 h/\partial x^4)$ [29, 30], where the parameter B is equal to $D\gamma C/n^2 k_B T$ in which D is the surface diffusivity, γ is the surface free energy, C is the concentration of mobile species, and n is the areal concentration of atomic sites. Makeev [1] extended the BH sputtering mechanism to include higher order effects of the ion–surface interaction which are manifested as additional terms of the form $B_I \partial^4 h/\partial x^4$ due to the ion–surface interaction.

The simultaneous action of these roughening and smoothing processes can be used to derive a linear equation for the evolution of the surface height ($h(x, y, t)$):

$$\frac{\partial h}{\partial t} = -v_0 + \frac{\partial v_0}{\partial \theta}\frac{\partial h}{\partial x} + v_x \frac{\partial^2 h}{\partial x^2} + v_y \frac{\partial^2 h}{\partial y^2} - B\nabla^2\nabla^2 h - B_{I,x}\frac{\partial^4 h}{\partial x^4} - B_{I,xy}\frac{\partial^4 h}{\partial x^2 \partial x^2} - B_{I,y}\frac{\partial^4 h}{\partial y^4}. \quad (1)$$

This predicts that each Fourier component of the surface height ($h_k(t)$) will grow (or shrink) exponentially with an amplification factor (r_k) that depends on the wavevector:

$$r_k = -v_x k_x^2 - v_y k_y^2 - B(k_x^2 + k_y^2)^2 - B_{I,x}k_x^4 - B_{I,xy}k_x^2 k_y^2 - B_{I,y}k_y^4 \quad (2)$$

r_k has a maximum value of r^* at a wavevector k^* given by

$$k^* = \left(\frac{v_{max}}{2\left(B + B_{I,max}\right)}\right)^{1/2}, \quad (3a)$$

and

$$r^* = \left(\frac{v_{max}^2}{4\left(B + B_{I,max}\right)}\right) \quad (3b)$$

where max is the direction (x or y) that corresponds to the fastest growing wave vector. In addition, the linear theory also predicts that the ripples will travel across the surface for modes with k^* parallel to the ion beam direction on the surface.

These predictions are based on the linear equation above; other non-linear terms have been proposed to account for features of pattern formation outside the linear model described

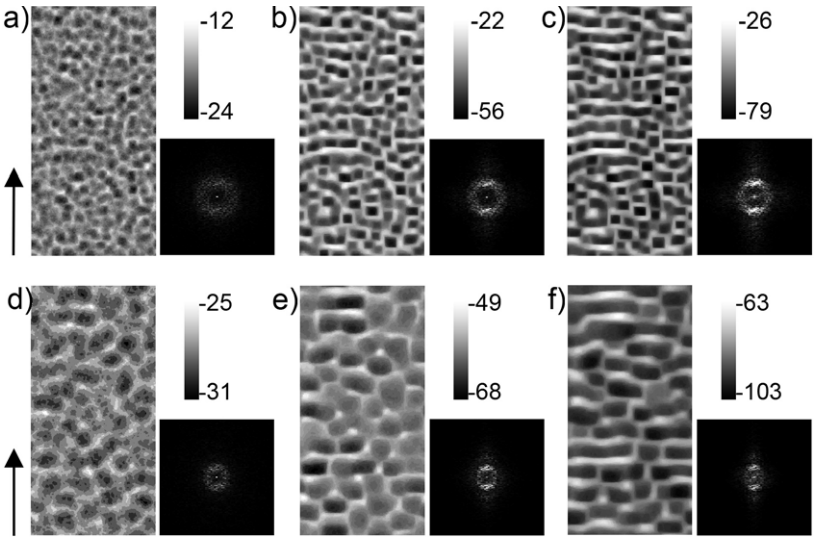

Figure 3. Morphology of the surface at different times during the sputtering simulation. (a)–(c) images correspond to removal of 20, 40 and 60 ML at temperature of 187 °C. (d)–(f) images correspond to removal of 30, 60 and 90 ML at temperature of 250 °C. The scale next to each figure relates the gray level to the surface height in units of the simulation lattice parameter. The power spectral density of the surface is shown below each image of the surface.

here [1]. We focus on the linear terms because these provide predictions for features such as the ripple wavelength and growth rate that can be compared directly with the simulation results.

4. Simulation results

In the following sections, we present the results of our simulations for ripple formation produced using a range of fluxes and temperatures. We analyze the simulated surface morphology to obtain quantities that can be compared directly with the continuum model and with experiments: ripple wavelength, growth rate and lateral velocity. The results are compared quantitatively with the predictions of the linear instability theory in order to determine how well the continuum model describes the results of the atomistic simulations. In addition, we compare the results with relevant experimental studies to understand how well the numerical approaches capture the actual physical behavior. In section 5, we summarize the deviations among the continuum calculations, simulations and experiments in order to discuss what they tell us about how patterns form on ion bombarded surfaces.

4.1. Ripple morphology and time evolution

Some typical surface morphologies resulting from the simulations are shown in figure 3 (the ion beam parameters used are $a = 20$, $\sigma = \mu = 10$, and sputter yield $= 2$, with all the lengths measured in units of the lattice spacing, a_0). The images represent surfaces after simulated sputtering at temperatures of 187 °C for removal of 30, 60 and 90 monolayers (ML) (figures 3(a)–(c)) and 250 °C for removal of 20, 40 and 60 ML (figures 3(d)–(f)); the ion flux f is 2 ML s^{-1}. The gray scale corresponds to the height at each surface position as shown on the accompanying marker. The patterning

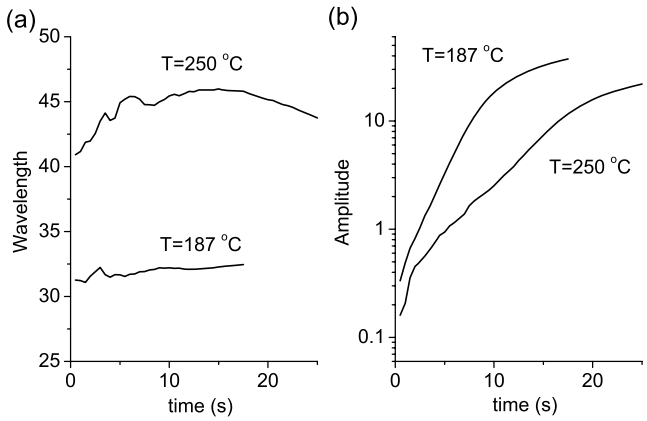

Figure 4. Evolution of the (a) wavelength and (b) amplitude of the ripple pattern during sputtering simulation. The temperature is indicated in the figure.

behavior is apparent in the morphology that develops on the simulated surface. Adjacent to each image is the PSD of the surface height; the peak in the PSD confirms the presence of a preferred periodicity on the surface. The wavelength and amplitude of the ripple are determined from the position and magnitude of the peak in the PSD for each simulated surface morphology.

The evolution of the characteristic ripple wavelength and amplitude are shown in figures 4(a) and (b) for the same conditions used in figure 3. The wavelength and amplitude are given in units of the surface lattice parameter a_0. In the early stages, the ripple amplitude is seen to grow exponentially with sputtering time. During this growth, the corresponding wavelength is essentially constant with a well-defined peak in the PSD. In addition, the orientation of these ripples is defined by the ion beam direction; when the azimuthal orientation of the beam is changed in the simulation, the orientation of the

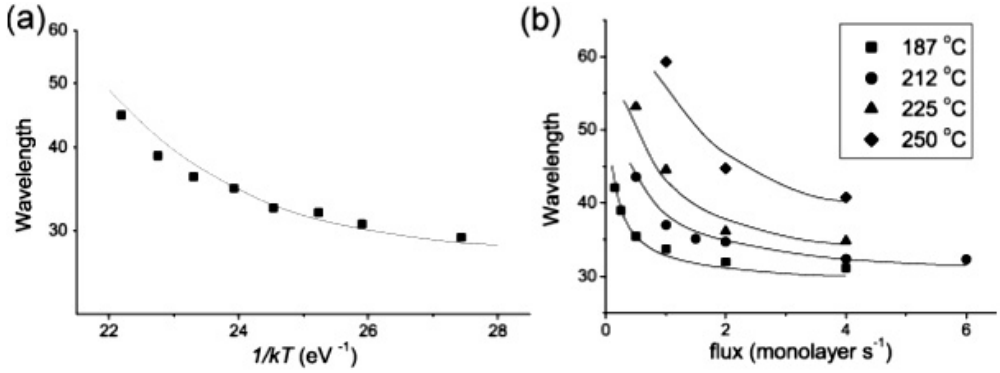

Figure 5. Dependence of the simulated ripple wavelength on (a) temperature at a flux of 2 ML s^{-1} and (b) flux at different temperatures as indicated in figure. Solid lines represent fit to linear instability theory evaluated using measured value of surface defects. Reprinted from [10] with permission. Copyright 2006 by the American Physical Society.

pattern changes as well [31]. The exponential growth, fixed wavelength and sample orientation are all features of the linear instability mechanism as predicted by the BH theory. After extended periods, the amplitude saturates which signals the end of the region over which the behavior can be compared with the linear model and indicates the onset of non-linear behavior.

4.2. Dependence of wavelength on flux and temperature

The temperature dependence of the wavelength for the simulated ripples is shown in figure 5(a) on an Arrhenius plot for an ion flux of 2 ML s^{-1}. The plot is not linear, indicating that λ is not controlled by a single activated process. The apparent activation energy (i.e., the slope of $\ln(\lambda)$ versus $1/kT$) is larger at high temperature while at low temperature, the slope becomes very shallow. The flux dependence of the wavelength also changes with temperature, as shown in figure 5(b). At the higher temperatures studied, the wavelength is inversely proportional to the flux. At lower temperature, the wavelength is weakly dependent on the flux over most of the range studied, only increasing at the lower range of fluxes studied.

The BH model predicts the flux and temperature dependence of the ripple wavelength to be:

$$\lambda^* = 2\pi\sqrt{\frac{2(B + B_{I,\max})}{\nu_{\max}}} \propto \sqrt{\frac{D(T)C(f,T)}{fT} + A_I} \qquad (4)$$

where the f and T dependence of each of the parameters is shown explicitly to illustrate its effect on the resulting ripple formation. $D(T)$ refers to the diffusivity of the mobile defects which is equal to $\Gamma \exp(-E_D/kT)$ in the simulations. Although the activation energy for surface vacancies and adatoms can be chosen independently, we use the same value of 0.8 eV for both in the simulation results discussed here. Since both B_I and $\nu_{\max}$ depend linearly on flux, the ratio $A_I = B_I/\nu_{\max}$ is independent of flux.

In order to evaluate this equation, we also need to know the concentration of the mobile defects, $C(f,t)$. This depends on both temperature and flux since it is controlled by the kinetic balance between creation of defects (by ion-induced and thermal processes) and annihilation of defects (at sinks such as step edges and clusters or via recombination). Conveniently (and unlike experiments), the average concentration can be evaluated directly by counting the number of adatoms and surface vacancies on the simulated surface. Although this ignores the possible effects of gradients in the defect concentration correlated with the surface morphology, these are believed to be small based on the observed uniformity of the surface defect concentration.

The average surface defect concentration remains fairly constant and uniform over the regime in which the ripples grow exponentially. The defect concentration as a function of time (figure 6(a), $T = 187\,^{\circ}$C, $f = 1$ ML s^{-1}) indicates that the majority of the mobile defects are surface vacancies, consistent with the fact that sputtering via the Sigmund mechanism only creates vacancy-like defects in our simulation (the effect on the surface morphology of forming additional adatom and surface vacancy defects from Frenkel pair creation is discussed in section 4.6.2). Although the processes controlling the defect concentration are complex, the data over all the simulations studied is found to scale as $C \sim (f/D)^{1/2}$ (figure 6(b)) over the range of parameters studied.

We fit the simulation results to equations (4) to determine the agreement with the BH theory predictions. The only parameters needed for the fitting are the value of the activation energy for the defect diffusivity (E_D), the ratio A_I and an overall scaling constant. The value of the defect concentration was not a fitting parameter but was instead taken from the actual concentration measured on the surface during the simulation. The BH prediction for the amplification factor can be obtained from the same kinetic constants (described below) so that all the simulation data was fit using a single set of fitting parameters. The value for the activation energy determined from the fitting procedure is 0.86 eV, in good agreement with the value of 0.8 used as input to the simulation. The value for A_I is equal to 709 a_o^2 which corresponds to a wavelength of 26.6 a_o in the absence of thermal diffusion. Based on the sputtering parameters used in our simulation, the wavelength predicted by the continuum theory is 25.7 a_o when thermal diffusion is absent.

Comparison of the simulation with the BH predictions for λ is shown as the solid lines in figure 5. The continuum

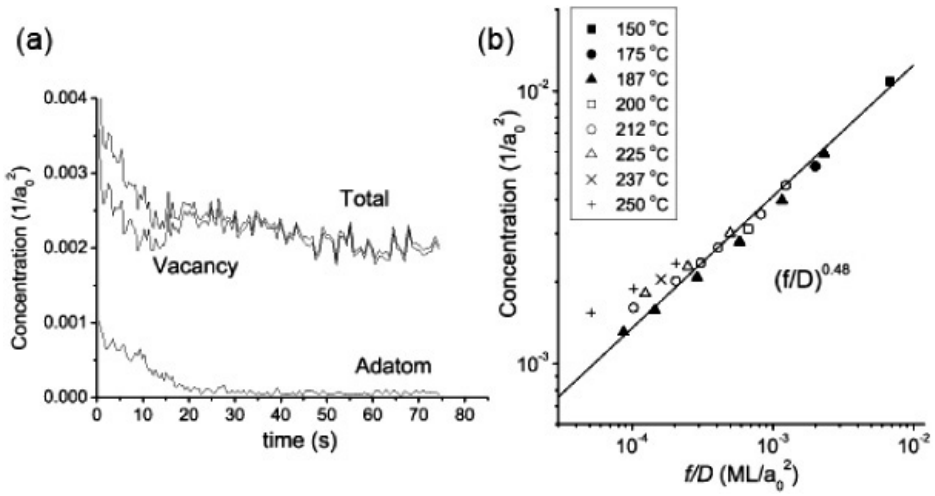

Figure 6. (a) Evolution of surface defect concentration (adatoms, vacancies) with sputtering time in KMC simulations. (b) Dependence of average simulated total defect concentration on f/D from simulations conducted at different temperatures and fluxes. Reprinted from [10] with permission. Copyright 2006 by the American Physical Society.

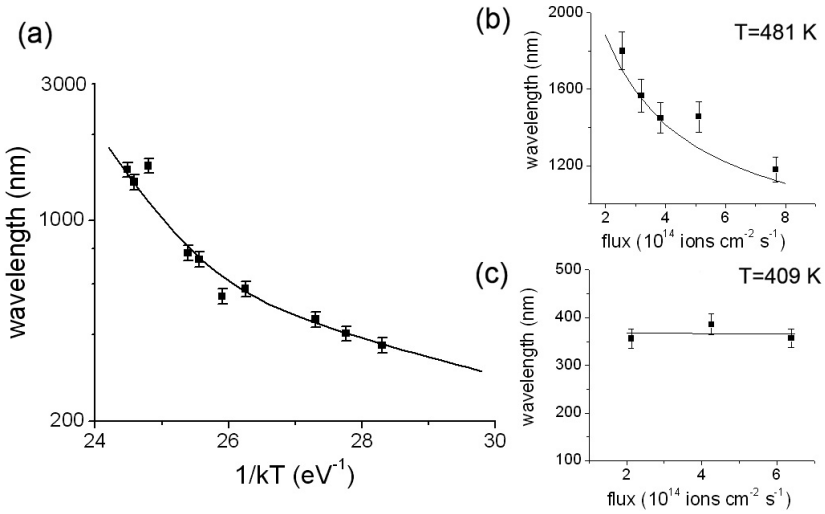

Figure 7. Wavelength of sputter ripple measured on Cu(001) surface as a function of (a) temperature at constant flux and as a function of flux at (b) temperature = 481 K and (c) temperature = 409 K. Solid line is fit to linear instability theory using analytical model for defect concentration. Reprinted from [33] with permission. Copyright 2005 by the American Physical Society.

model is able to explain the full range of flux and temperature dependence seen in the simulation due to the balance between the thermal and the ion-induced terms in equation (4). At high temperatures, the temperature dependence of the wavelength is dominated by the thermally-activated diffusivity so that the apparent activation energy is comparable to E_D. At low temperatures, the wavelength approaches a constant determined by the value of A_I so that the slope of the Arrhenius plot decreases. The trends for the simulated wavelength with flux are equally well modeled. At lower fluxes or higher temperatures ($DC/fT \gg A_I$), the thermally-controlled processes dominate and the enhanced smoothing leads to an increase in the ripple wavelength. At high fluxes ($DC/fT \ll A_I$), the wavelength approaches the asymptotic value determined by the ion-induced smoothing. The good agreement seen here between the simulations and the linear instability model suggests that the continuum model can adequately explain many features of ripples produced by the Sigmund sputtering mechanism.

In addition to comparing the simulations with the BH model, it is useful to see how both compare with actual experimental results. Therefore, similar to the KMC simulations, we have measured the wavelength and amplification factor during sputtering of Cu(001) surfaces [32, 33]. The measurements were performed in kinetic regimes in which the pattern formation had features of the BH ripples, i.e., the wavelength was essentially constant during the sputtering, the amplitude grew exponentially and the orientation was determined by the ion beam. The wavelength of the ripples on the Cu surface is shown as a function of temperature in figures 7(a) and as a function of flux for two different temperature in figures 7(b) and (c). The experiments

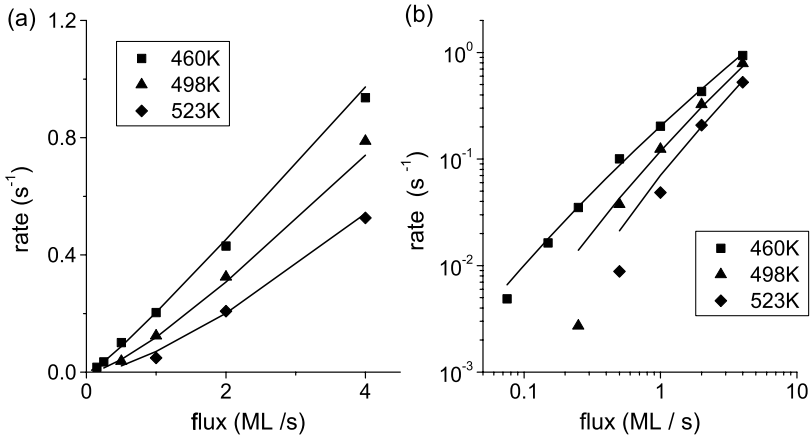

Figure 8. Dependence of amplification factor of simulated ripples on the flux on (a) linear plot and (b) log plot. The simulations deviate from the linear instability theory (solid line) as the flux decreases. Reprinted from [10] with permission. Copyright 2006 by the American Physical Society.

share some qualitative features with the KMC simulations: the temperature dependence is not simply Arrhenius and the flux dependence of the ripples changes with the temperature.

In the experiments, unlike the simulations, we cannot determine the defect concentration directly to allow comparison with the BH model. Instead, Chan *et al* [33] developed a simple kinetic model that included defect formation by ion bombardment and also by thermal mechanisms. At high temperature, the defect concentration is thermally generated (independent of flux) while at low temperature it is generated by the ion beam (proportional to the flux). Incorporation of this flux- and temperature-dependent defect concentration into the BH calculations produces the results shown as the solid lines in the figures which agree well with the experimental data.

Although the f and T dependences are qualitatively similar, it is important to note that the kinetic regime of the experiments is not the same as in the simulations. In the KMC results, the dependence of the wavelength was based on a competition between thermal smoothing and ion-induced athermal smoothing. The defect concentration was found to depend on $(f/D)^{1/2}$ and not have the temperature dependence predicted by Chan's model. Computational speed limited the range of defect kinetics that could be accessed, so the KMC could not simulate the ripple formation in the same regime that the experiments were done in. However, it should be noted that experiments on Cu(001) at low temperature [34] find a ripple wavelength that is independent of the wavelength, as seen in the simulations.

4.3. Dependence of r^* on flux and temperature

The growth rate of the ripples is obtained from the time evolution of the amplitude in the exponential growth regime. From this we extract the amplification factor r^* which we use to characterize the ripple growth and to compare directly with the predictions of the instability theory. The results for r^* from the simulations under different flux and temperature conditions are shown in figure 8(a) on a linear scale. For each temperature, the amplification factor increases with the ion flux. For the same flux, the growth rate is larger at low temperatures than at high temperatures. This trend in the growth rate is correlated with the wavelength so that ripples with shorter wavelength grow faster than ripples with long wavelength. The growth rate appears to go to zero at a critical flux for each temperature, with the critical flux being larger at higher temperatures. Shown on a logarithmic scale in figure 8(b), there is a rapid drop in the amplification factor as the flux is decreased.

The BH model predicts the dependence of the amplification factor on flux temperature in the same way as for the wavelength:

$$r* = \frac{\nu_{\max}^2}{4\left(B + B_{I,\max}\right)} \propto \frac{f}{\left(\frac{D(T)C(f,T)}{fT}\right) + A_I}. \qquad (5)$$

The fitting parameters were obtained by simultaneously fitting the wavelength data and the growth rate data and using the measured values for the defect concentration. Results of the BH model calculations for the ripple amplification rate are shown by the solid lines in figure 8(b). The model and simulations agree well when $DC/fT \approx A_I$ (at high fluxes or low temperatures). At lower fluxes or higher temperatures ($DC/fT \ll A_I$), however, the model and the simulation results diverge. The BH model predicts that r^* is proportional to $f^{3/2}$ if the scaling of $C \sim (f/D)^{1/2}$ found in the simulations is used. This value of r^* found in the simulations is significantly lower than the value predicted by equation (5) (solid line in figure 8(b)) in the low flux regime. In the simulations, at low flux there is a transition to non-roughening behavior so that the ripples grow much slower than predicted by the BH theory or not at all within the simulated time.

For comparison with real physical systems, the growth rate of the ripples was also measured on Cu surfaces as a function of flux and temperature [32]. The results (figure 9) indicate that the amplification factor increases with larger flux and at lower processing temperatures, similar to the results of the simulations. For both temperatures, the amplification factor does not go smoothly to zero but appears to vanish below a critical flux value.

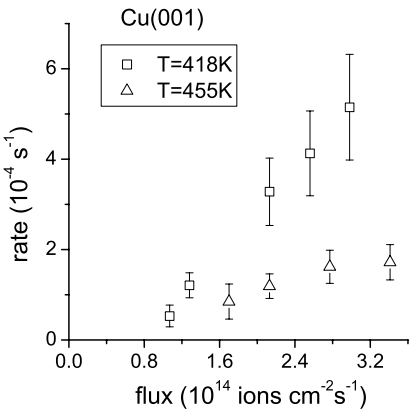

Figure 9. Amplification factor of sputter ripples measured on Cu(001) surface as a function of flux at temperatures of 418 and 455 K. Reprinted from [3] with permission. Copyright 2007, American Institute of Physics.

4.3.1. Transition to non-roughening behavior. The rapid decline in the growth rate at low fluxes is seen in both the simulations and the experiments, but is not consistent with the linear instability mechanism which predicts that the amplification factor should go smoothly to zero with decreasing flux. We attribute this discrepancy to a significant difference between the assumptions of the continuum model and the actual system. In the continuum model, the transport on the surface is modeled by the Mullins–Herring theory which ignores the effect of steps on the surface. The success of the BH model in predicting the wavelength and the amplification factor on flux and temperature indicates that this is an acceptable simplification over a wide range of conditions. However, when the flux is low or the temperature is high, this approximation becomes most problematic. For a crystal surface under the roughening-transition temperature to roughen, new terraces must be nucleated on the surface. In the low flux and high temperature regime, where the ion-induced damage is quickly recovered by thermal diffusion, new terraces can not be created. Instead of forming ripples, the surface will be eroded by layer-by-layer removal. Indeed, a transition to oscillation in the rms roughness (a signature of layer-by-layer erosion) is observed for the simulations at the point where the roughening rate deviates from the continuum model prediction.

Similar transitions from layer-by-layer to roughening are seen during growth. A theoretical model for this transition in the presence of ES barriers is given by Tersoff [35]. However, we find the transition in our simulations occurs even without an ES barrier.

4.4. Relationship between amplification factor and wavelength

The preceding analysis of the wavelength and amplification factor in terms of the continuum model relied on knowing the concentration of mobile defects contributing to relaxation of the surface roughness. In the linear instability model, however, the wavelength and amplification factor are intimately tied together so that

$$\frac{r^*}{f} = \frac{1}{2}\frac{\nu_{\max}}{f}k^{*2} \tag{6}$$

where $k^* = 2\pi/\lambda^*$. Since $\nu_{\max}/f$ is a constant that depends only on the ion parameters, the relationship between the wavelength and the amplification factor expressed in this way is independent of the defect kinetics or the surface smoothening rate B, i.e., r^* and k^* can be determined and the relationship between them evaluated without knowing anything about the defect diffusivity or concentration. This is especially useful for evaluating experimental results where the defect kinetics are not necessarily known.

The relationship between r^* and k^* from the simulated ripples (figure 10) shows a clear dependence of the amplification factor on k^{*2} over a wide range of simulation conditions. The value for $\nu_{\max}/f$ obtained from fitting the curve to k^{*2} behavior agrees within 25% with the value calculated from the ion beam parameters. For comparison with experiments, similar measurements of r^* versus k^* made on Cu(100) surfaces are shown in figure 10(b) [3]. The scatter is significant but the data is not inconsistent with a k^{*2} behavior. However there is significant disagreement between the value of $\nu_{\max}/f$ obtained from fitting this data with the value expected from the BH theory. Using values for the ion parameters obtained from SRIM [36], the calculated value of $\nu_{\max}/f$ is 200 times less than the experimental value. In other words, the ripples in the experiments grow with an amplification factor that is 200 times larger than predicted by the BH theory. Although the parameters obtained from SRIM may not be entirely accurate, it is doubtful that they could be incorrect by a large enough margin to account for this discrepancy.

This suggests that there may be other roughening mechanisms at work in real systems that are not included in the continuum model or simulations. One candidate is that the surface modification by the ion is more complex than in the Sigmund model. For example, Kalyanasundaram *et al* [15] have shown with MD simulations that there is significantly more surface transport induced by the ion beam than accounted for by the Sigmund sputtering. Other possible sources of additional roughening are the presence of ES diffusion barriers or the creation of multiple defects by the ion beam (discussed in section 4.6). In addition, recent measurements have shown that the ion–surface interaction can create significant surface stress that may also act as a driving force for surface patterning [37].

4.5. Velocity of ripples

The BH theory predicts that the ripples that form with the wavevector parallel to the ion beam direction should travel along the surface [1]. The velocity is determined by the dependence of the sputter yield on the angle of incidence. By carrying out the ion–solid interaction to higher order, Makeev also calculated the dispersion of the ripple velocity, i.e., how it depends on the surface wavevector. The ripples produced by the KMC simulation do in fact travel across the surface as predicted by the BH theory. We find that there is excellent agreement between the predictions of the instability model and the measured ripple velocity in the simulation [3].

Recently, experiments have been performed in which the ripple velocity was measured directly on the surface [38, 39].

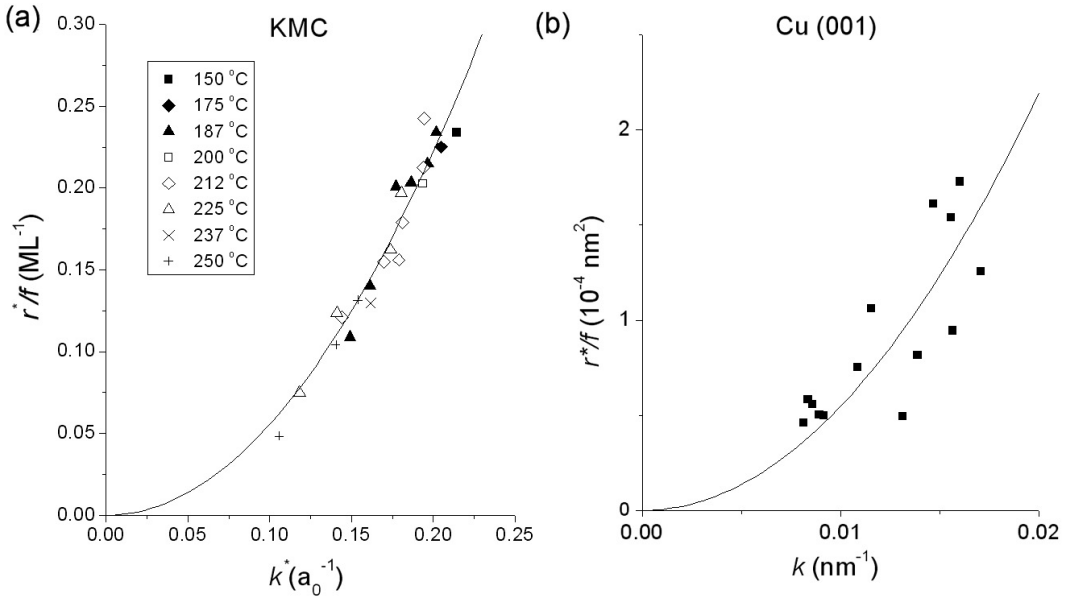

Figure 10. Relationship between normalized amplification factor (r^*/f) and ripple wavevector for (a) simulations and (b) Cu(001). Solid lines are fit to k^{*2} dependence predicted by the linear instability theory. Reprinted from [3] with permission. Copyright 2007, American Institute of Physics.

Surprisingly, these experiments find that the ripple travels in a direction opposite to the direction predicted by the BH theory. Because of the excellent agreement between the simulations and the BH theory, the discrepancy does not appear to be in the formulation of the velocity in the continuum model. Rather it suggests that there may be other mechanisms at work controlling the traversal of ripples across the surface. For example, Alkemade [39] has suggested that inhomogeneous viscous flow on amorphous surfaces may account for the measured velocity. However, it is important to note that these experiments were done with FIB instruments in which the effects of Ga incorporation and rastering of the ion beam may play a role. In addition, the surfaces studied were Si in which the surface is amorphized by the beam.

4.6. Additional effects: ES barriers and multiple defects

An important question in the formation of ion-induced patterns is why the patterns observed experimentally appear to grow more quickly than predicted by the BH theory (as discussed in section 4.4). In the following section, we use the simulations to consider the effects of ES barriers and multiple defect formation by the ion beam on the formation of patterns and to determine their relationship to the rapid roughening that has been observed.

4.6.1. ES barrier. The ES barrier can also serve as a driving force for pattern formation during ion bombardment [2, 40]. In these cases, the pattern aligns with the crystallographic direction and the wavelength is often found to increase with sputtering time. A number of simulations have been devoted to studying the roughening induced by the ES barrier [25–28], but these do not include the Sigmund sputtering mechanism ([24] includes both the Sigmund mechanism and ES barriers). Different roughening mechanisms can dominate in different kinetic regimes on a single material surface so that, for instance, BH ripples form at high flux and high temperature but ES-induced ripples form at lower temperatures or fluxes [41]. In order to study the interplay between these mechanisms, we have studied the effect of adding an ES barrier to our KMC simulations. The barrier is added uniformly to the activation energies for all processes that involve interlevel transitions. For a barrier of zero height, the simulation is identical to the results described previously. We only give a brief summary of our preliminary findings here; detailed results will be presented in a future publication.

When we increase the barrier from 0 to 0.1 eV, we clearly observe a transition from a 1d ripple morphology (like that shown in figure 3) to a bi-directional roughening that follows the symmetry of the surface. The roughening kinetics changes from an exponential behavior to a power law behavior with a faster roughening rate; some experiments and previous simulations also observe a power law increase in roughness when the ES barrier is dominant. We also find that the ES barrier itself is not the main cause for coarsening of the wavelength observed in experiments. Instead, patterns are found to coarsen as we decrease the barrier for edge diffusion, in agreement with similar findings reported in other KMC simulations [25, 28].

Valbusa [2] has suggested that in the early stages of patterning, the ES barrier modifies the linear instability theory by adding a term proportional to the surface curvature ($S_x\partial^2 h/\partial x^2 + S_y\partial^2 h/\partial y^2$), similar in form to the BH roughening term but having its origin in repulsion by the ES barrier at the step edges. This term has the effect of increasing the wavevector and amplification factors in equations (3) by replacing $\nu_{\max}$ with $\nu_{\max} + S_{\max}$. The simulations indicate that the ripples do indeed grow faster and have a shorter wavelength

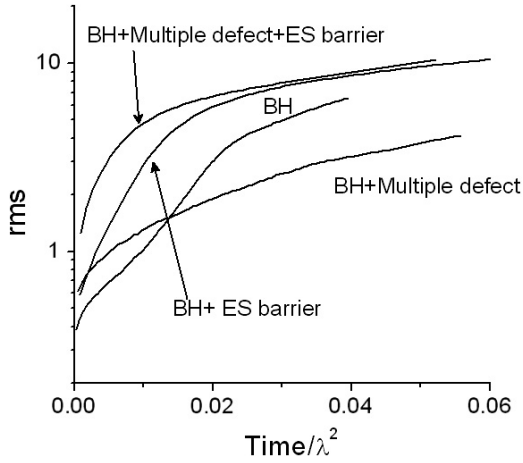

Figure 11. Evolution of ripple amplitude with time showing effects of including multiple defects per ion and adding an ES barrier to the interlevel transitions.

when both the ES barrier and Sigmund mechanism are present, as predicted by this model. However, since an exponential growth regime can no longer be identified as the ES barrier increases, it appears that a linear model is insufficient to explain the induced roughening.

For comparison, figure 11 shows the evolution of the RMS roughness with time for the case of the sputtering mechanism alone (BH) and with the addition of the ES barrier (BH + ES barrier). The time is divided by the square of the wavelength to compare the roughening rate for different mechanisms after eliminating the effects due to changing the wavelength. The simulations show that the roughness grows faster with the addition of the ES barrier, even when the change in the wavelength is accounted for. However, we also find that the ES barrier is more effective in increasing the average RMS roughness than the correlated roughness. In other words, the patterns induced by the Sigmund mechanism have a more well-defined wavelength and greater long-range order relative to the patterns produced with the addition of the ES barrier. If only the growth of the ripple amplitude is monitored (i.e., the magnitude of the PSD at the ripple wavelength), then the roughening rate does not appear to increase due to the addition of the ES barrier.

Based on these preliminary results, it is not clear that the effect of the ES and BH roughening mechanisms can be superimposed in a linear instability model. The roughening induced by one mechanism does not appear to be independent from the roughening induced by the other and significant couplings between the different roughening and relaxation mechanisms may come into play.

4.6.2. Multiple defects. In the simulation results discussed up to this point, the sputtering mechanism was only allowed to create surface vacancy defects as described in the Sigmund model. However, it is known that multiple defects (adatoms and vacancies) are created by ion bombardment. In the following section we discuss the results of extending the sputtering mechanism to include the creation of multiple defects for each ion. For the results presented, the ion beam parameters used are: for sputtering: $a = 15, \sigma = \mu = 7.5$, and sputter yield $= 2$; for multiple defects: $a = 15, \sigma = \mu = 7.5$ (vacancy) and $a = 15, \sigma = \mu = 15$ (adatom), and number of vacancy/adatom pairs $= 8$. All the simulation are run at $T = 225\,^{\circ}\mathrm{C}$ and $f = 1\ \mathrm{ML\ s^{-1}}$.

In the multiple defect model, we consider the effect of creating Frenkel pairs consisting of vacancies and interstitials below the surface in addition to the surface vacancies created by sputtering. These defects are generated inside the bulk around the ion trajectory using the same approach as used for calculating the sputtering, i.e., the probability of creating the defect is proportional to the energy deposited at different sites. The probability distribution used for simulating the vacancies is the same Gaussian as the one used to determine the position of the sputter atoms (i.e., as shown in figure 2). The Gaussian used for interstitials (the counterpart of adatoms in the bulk) is concentric with that used for the vacancy calculation, but with a width that is two times larger. This accounts for the observation that interstitials are usually created further away from the stopping point of the ion. The bulk defects are propagated probabilistically to surface sites, using a probability proportional to $\exp(-r^2/2d^2)$, where r is the distance between the bulk defects and the surface site and d is the depth of the bulk defect. Based on this calculation, the surface site is either increased in height (corresponding to a bulk interstitial becoming an adatom) or decreased in height (corresponding to bulk vacancies becoming surface vacancies). Using this approach, surface vacancies are concentrated at the center with adatoms surround them, mimicking the defect distribution observed in experiments and simulations. In addition, similar to the Sigmund mechanism, the positions of the surface defects depend on the local surface morphology.

For comparison with the previous results, we simulated surface evolution with the creation of eight pairs of adatoms and vacancies in addition to the surface vacancies created by the Sigmund sputtering mechanism. The surface morphology was similar to that produced under the same conditions with only sputter-induced surface vacancies. In figure 11, we can see that adding the multiple defects alone actually lowers the roughening rate (BH + multiple defects) relative to the BH mechanism alone. This is possibly due to the rapid recombination of the single adatoms and vacancies after their creation, which makes it so that the additional defects do not contribute to increasing the roughening.

Since the recombination of defects is slower in the presence of ES barrier, we have also run the multiple defect simulation with the ES barrier (BH + multiple defects + ES barrier in figure 11). After adding the ES barrier, the wavelength of the pattern is reduced and there is a significant increase in the apparent roughening rate. The above results suggest that multiple defects can enhance roughening if they are not readily recombined. Finally, we note that we do not include the creation of craters and adatom clusters. Since clusters are immobile as compared to the single surface defects and they are more difficult to recombine, we expect that adding defect clusters will enhance the roughening rate.

5. Summary

The KMC simulations indicate that the combination of curvature-dependent sputtering based on the Sigmund model with thermally-activated defect diffusion can produce surface patterns similar to those predicted by the BH theory and the linear instability mechanism. The ripples grow exponentially, with a fixed wavelength and a direction determined by the ion beam direction. Quantitative analysis of the relationship between the characteristic features of the ripples in terms of the BH model show good agreement in many respects. When the defect concentration measured in the simulations is used to evaluate the kinetic parameters, the flux and temperature dependence of the wavelength, growth rate and velocity agree with the predictions of the continuum theory. This validates that the BH model is a good continuum approximation of the surface evolution due to these mechanisms. This appears to be true even though there are significant assumptions of the BH model that are not true on the simulations, e.g., the Mullins–Herring diffusion ignores the effects of surface steps even though they are present in the simulation. This may account for some of the differences between the simulations and the continuum model such as the transition to non-roughening behavior at low fluxes or high temperatures.

Comparison of the simulation and continuum results with experiments on Cu surfaces also illuminates areas of agreement and disagreement with the instability model. The flux and temperature dependence of ripple wavelength and growth rate are qualitatively similar to the simulations, i.e., the temperature dependence of the wavelength is non-Arrhenius and the flux dependence changes with the temperature. Furthermore, the flux dependence of the growth rate is similar between the simulations and experiments, including a transition to non-roughening behavior at low fluxes. However, analysis with the BH model indicates that the regime of the surface kinetics is different between the experiments and the simulations. The defect concentration in the simulations scales like $(f/D)^{1/2}$ over the entire range of parameters whereas the experiments can be explained by a defect model that contains thermally-generated defects at high temperature and ion-induced defects at low temperature.

Furthermore, there are significant differences between the experiments and the simulations that point to areas where additional mechanisms need to be considered. The growth rate of the ripples in experiments on Cu is significantly faster than predicted by the BH theory. This may indicate the presence of additional toughening mechanisms (such as non-Sigmund sputtering or ion-induced stress) that enhance the ripple growth rate. The ripple velocity in experiments on Si is the opposite of that predicted by the BH theory, indicating there may be other surface transport mechanisms that require consideration. Finally, many features of the ripple growth in the later stages (amplitude saturation, coarsening) and under other conditions (quantum dot growth at normal incidence [42]) are outside of the scope of the linear instability mechanism and need more complex non-linear theories in order to be understood. In summary, the simulations indicate that there is validity to the BH mechanism but highlight the fact that there are many additional mechanisms that need to be considered.

Acknowledgments

We gratefully acknowledge many helpful discussions and input from Vivek Shenoy and M S Bharathi. The work is supported by US Department of Energy under Contact DE-FG02-01ER45913.

References

[1] Makeev M A, Cuerno R and Barabasi A L 2002 *Nucl. Instrum. Methods* B **197** 185
[2] Valbusa U, Borangno C and de Mongeot F R 2002 *J. Phys.: Condens. Matter* **14** 8153
[3] Chan W L and Chason E 2007 *J. Appl. Phys.* **101** 121301
[4] Munoz-Garcıa J, Vazquez L, Cuerno R, Sanchez-Garcıa J A, Castro M and Gago R 2008 *Self-Organized Surface Nanopatterning by Ion Beam Sputtering* (*Lecture Notes on Nanoscale Science and Technology*) ed Z Wang (Heidelberg: Springer)
[5] Bradley R M and Harper J M E 1988 *J. Vac. Sci. Technol.* A **6** 2390
[6] Cuerno R and Barabasi A L 1995 *Phys. Rev. Lett.* **74** 4746
[7] Makeev M A and Barabasi A L 1997 *Appl. Phys. Lett.* **71** 2800
[8] Park S, Kahng B, Jeong H and Barabási A-L 1999 *Phys. Rev. Lett.* **83** 3486
[9] Castro M, Cuerno R, Wázquez L and Gago R 2005 *Phys. Rev. Lett.* **94** 016102
[10] Chason E, Chan W L and Bharathi M S 2006 *Phys. Rev.* B **74** 224103
[11] Chason E and Dodson B W 1991 *J. Vac. Sci. Technol.* A **9** 1545
[12] Sigmund P 1969 *Phys. Rev.* **184** 383
[13] Sigmund P 1973 *J. Mater. Sci.* **8** 1545
[14] Floro J A, Kellerman B K, Chason E, Picraux S T, Brice D K and Horn K M 1995 *J. Appl. Phys.* **77** 2351
[15] Kalyanasundaram N, Ghazisaeidi M, Freund J B and Johnson H T 2008 *Appl. Phys. Lett.* **92** 131909
[16] Davidovitch B, Aziz M J and Brenner M P 2007 *Phys. Rev.* B **76** 205420
[17] Morgenstern M, Michely T and Comsa G 1999 *Phil. Mag.* A **79** 775
[18] Hannon J B, Klunker C, Giesen M, Ibach H, Bartelt N C and Hamilton J C 1997 *Phys. Rev. Lett.* **79** 2506
[19] Cuerno R, Makse H A, Tomassone S, Harrington S T and Stanley H E 1995 *Phys. Rev. Lett.* **75** 4464
[20] Koponen I, Hautala M and Sievänen O-P 1997 *Phys. Rev. Lett.* **78** 2612
[21] Hartmann A K, Kree R, Geyer U and Kölbel M 2002 *Phys. Rev.* B **65** 193403
[22] Stepanova M and Dew S K 2004 *Appl. Phys. Lett.* **84** 1374
[23] Yewande E O, Hartmann A K and Kree R 2005 *Phys. Rev.* B **71** 195405
[24] Yewande E O, Kree R and Hartmann A K 2006 *Phys. Rev.* B **73** 115434
[25] Murty M V R, Cowles B and Cooper B H 1998 *Surf. Sci.* **415** 328
[26] Jacobsen J, Cooper B H and Sethna J P 1998 *Phys. Rev.* B **58** 15847
[27] Pomeroy J M, Jacobsen J, Hill C C, Cooper B H and Sethna J P 2002 *Phys. Rev.* B **66** 235412
[28] Strobel M, Heinig K-H and Michely T 2001 *Surf. Sci.* **486** 136
[29] Mullins W W 1959 *J. Appl. Phys.* **30** 77
[30] Herring C 1950 *J. Appl. Phys.* **21** 301
[31] Bharathi M S, Chan W L and Chason E, unpublished
[32] Chan W L, Pavenayotin N and Chason E 2004 *Phys. Rev.* B **69** 245413
[33] Chan W L and Chason E 2005 *Phys. Rev.* B **72** 165418

[34] van Dijken S, de Bruin D and Poelsema B 2001 *Phys. Rev. Lett.* **86** 4608
[35] Tersoff J, Denier van der Gon A W and Tromp R M 1994 *Phys. Rev. Lett.* **72** 266
[36] Marwick D J 1984–2000 *SRIM-2000.40* IBM Co., Yorktown, NY
[37] Medhekar N, Shenoy V B, Chan W L and Chason E 2009 *J. Phys.: Condens. Matter* at press
[38] Habenicht S, Lieb K P, Koch J and Wieck A D 2002 *Phys. Rev.* B **65** 115327
[39] Alkemade P F A 2002 *Phys. Rev. Lett.* **96** 107602
[40] Villain J 1991 *J. Physique* I **1** 19
[41] Chason E and Chan W L 2007 *Nucl. Instrum. Methods* B **256** 305
[42] Facsko S, Dekorsy T, Koerdt C, Trapper C, Kurz H, Vogt A and Hartnagel H L 1999 *Science* **285** 1551